To induce multiferroic behavior in a lead-free ferro/piezoelectric $Na_{0.5}Bi_{0.5}TiO_3$ (NBT)/$Co_{0.025}$ system through site specific cation engineering

Reported by Anita Kumari

A Dissertation Submitted to
Indian Institute of Technology Hyderabad
In Partial Fulfillment of the Requirements for
The Degree of Master of Science

भारतीय प्रौद्योगिकी संस्थान हैदराबाद
Indian Institute of Technology Hyderabad

Supervisor

Dr. Saket Asthana
Assistant Professor
Advanced Functional Materials Laboratory
Department of Physics
Indian Institute of Technology Hyderabad
April, 2013

Declaration

I declare that this written submission represents my ideas in my own words, and where others' ideas or words have been included, I have adequately cited and referenced the original sources. I also declare that I have adhered to all principles of academic honesty and integrity and have not misrepresented or fabricated or falsified any idea/data/fact/source in my submission. I understand that any violation of the above will be a cause for disciplinary action by the Institute and can also evoke penal action from the sources that have thus not been properly cited, or from whom proper permission has not been taken when needed.

Anita Kumari

(Signature)

(NAME - ANITA KUMARI)

(ROLL NO. - PH11M01)

ii

Approval Sheet

This thesis entitled **"To induce multiferroic behavior in a lead-free ferro/piezoelectric $Na_{0.5}Bi_{0.5}TiO_3$ (NBT)/$Co_{0.025}$ system through site specific cation engineering"** by **Ms. Anita Kumari** is approved for the degree of Master of Science from IIT Hyderabad.

Vandana Sharma (VANDANA SHARMA)

-Name and affiliation-

Examiner

Manish K (MANISH NIRANJAN)

-Name and affiliation-

Examiner

Saket Asthana (SAKET ASTHANA)

-Name and affiliation-

Adviser

_____

-Name and affiliation-

Co-Adviser

_____

-Name and affiliation-

Chairman

iii

Acknowledgements

In the beginning, I would like to say my deep sense of gratitude to Assistant Professor Dr. Saket Asthana Advanced Functional Materials Laboratory Department of Physics Indian Institute of Technology Hyderabad,-502 205 INDIA, for his generous and charitable guidance, help and useful suggestions. I am thankful to Karthik Thangavelu for his valuable suggestion and discussion at every step of my project work. I would like to express my sincere thanks to 'Physics research lab' members of IIT Hyderabad for their help and various suggestions.

I would like to say special thanks to my classmates Chandrima, Asmita, Swasti, Saptashwa, Mukesh, Sanjeev, Mujeeb for their unwavering support and for instilling confidence during the project. I would also like to thank Mrunalini B, Faby, Revathy, Anupama, Soumya, Annapurna, Akanksha and all my friends in IIT Hyderabad for making my stay at IIT Hyderabad, memorable and enjoyable.

Finally, I would like to thank my loving Grandfather and all family members for their complete constant support, patience, and love.

ANITA KUMARI

Dedicated to

My loving family

Abstract

Polycrystalline samples of $Na_{0.5}Bi_{0.5}TiO_3$ (NBT) and $Na_{0.5}Bi_{0.5}Ti_{0.975}Co_{0.025}O_{3\pm\delta}$ (NBT-Co) were prepared by using conventional solid state sintering technique. X-ray diffraction analysis showed single phase characteristics of both the samples. Further, it also gave an insight for the possibility of mixed oxidation states of Co-ion in the NBT host lattice, which is being well supported by the tolerance factor values. Magnetization measurements show a spin-glass like behavior for NBT-Co sample which is evident from the ZFC-FC plots. However, Co-ion substitution in NBT induces a paramagnetic behavior at room temperature and shows different signatures of magnetization curves below 50K. P vs. E Hysteresis measurements show improved Polarization values (P_r) and also with a slight hardening in the coercive field (E_C) for NBT-Co sample.

Contents

Chapter 1

Introduction

1.1 Introduction

Ceramics are defined as the solid compounds that consist of metallic and nonmetallic elemental solids which are formed by the application of heat and pressure or 'the art and science of making and using solid articles and are composed in large part of inorganic non-metallic martials '. In general the most common properties of ceramics are: hard, wear-resistant, brittle, thermal insulators, electrical insulators, nonmagnetic, oxidation resistance, thermal shock prone and chemically stable.[1] In present time ceramic materials are used everywhere.

Most of the materials are classified in terms of conductivity either as conductors and nonconductors, or technically as metals and insulators (or dielectrics). The electrical conductivity of a material usually depends on temperature and frequency. A material with high conductivity ($\sigma >> 1$) is called a metal whereas one with low conductivity ($\sigma << 1$) is called an insulator.[2]

1.2 Ferroelectricity:

There are seven crystal structures in 3-dimensional space. They are cubic, tetragonal, orthorhombic, rhomohedral (trigonal), hexagonal, monoclinic, triclinic. These systems can again be sub-divided into 14 Bravais lattices. Further, these 7 crystal systems are classified into 32 crystal classes known as point groups. Of the 32 crystal classes of materials, 11 possess centers of symmetry and hence possess no polar properties. Of the remaining 21, all but one exhibit all exhibit electrical polarity when subjected to a stress and hence are

called piezoelectric. Of the 20 piezoelectric crystal classes, 10 show a unique polar axis. These crystals are called polar because they possess a spontaneous polarization. Among them 11 points groups are centro-symmetric and so they do not possess any polarity.

Typically such a spontaneous polarization cannot be detected by the presence of charge on the surface of the crystal as free harge within the crystal flows to compensate the polarization. One can, however, often detect the presence of a spontaneous polarization by studying the temperature dependent changes in polarization which results in the flow of charge to and from the surfaces. This is known as the pyroelectric effect and these 10 polar crystal classes are often referred to as the pyroelectric classes. A material is said to be ferroelectric when it orients in two or more states in the absence of an electric field and can be shifted from one to another of these states by an electric field. Ferroelectric materials are invariant under time reversal symmetry, but must break spatial inversion symmetry. Ferroelectrics are materials that undergo a phase transition from a high-temperature phase that behaves as an ordinary dielectric to a low temperature phase which has a spontaneous polarization whose direction can be switched by an applied electric field. Any lattice of opposite point charges is inherently unstable and relies on short-range interactions between adjacent electron clouds in the material to stabilize the structure. In ferroelectric materials these interactions result in the formation of a double-well potential that stabilizes a distorted structure over the symmetric structure.

A material is said to be a ferroelastic when it has two or more orientation states in the absence of mechanical stress (and electric field) and can be shifted from one to another of these states by mechanical stress. It is imperative that two of the orientation states are identical in crystal structure and different in mechanical strain tensor at null mechanical stress (and electric field). The ferroelectric materials are a subgroup of pyroelectric materials in which polarization can be reversed. [3,4]

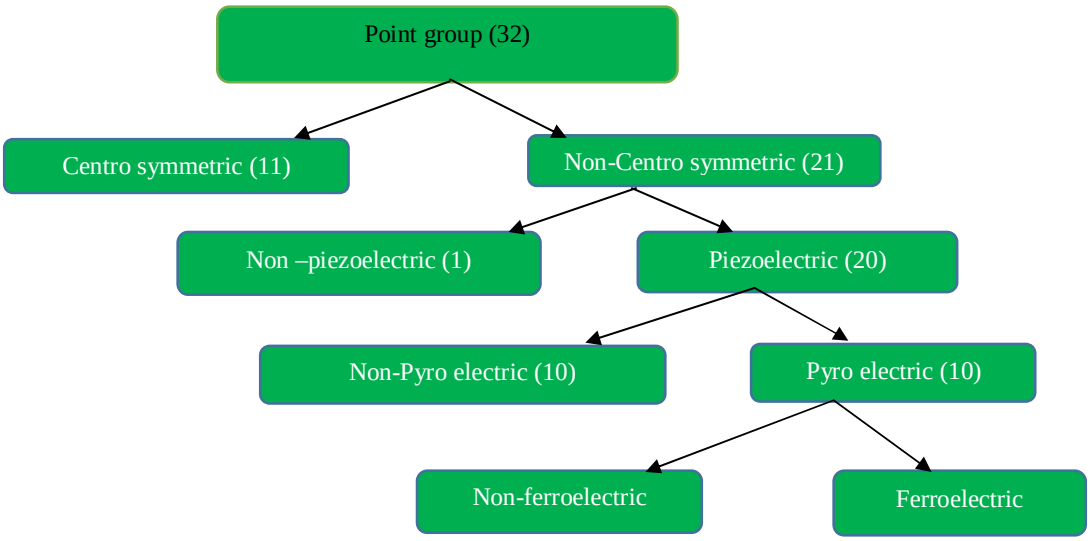

Fig. 1.1 Schematic representation of the classification of point groups

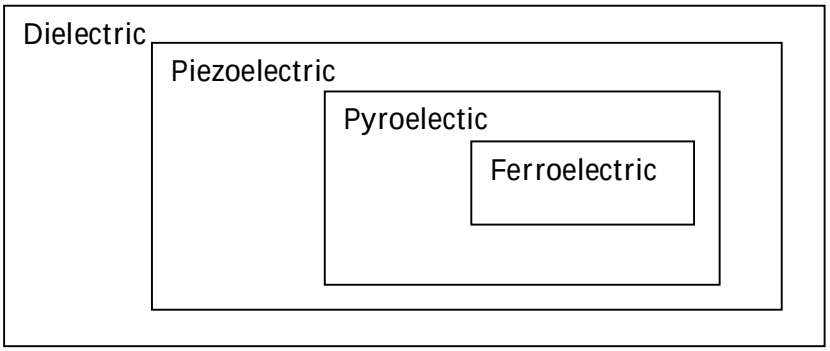

Fig.1.2 Diagrammatic representations of the relationship between ferroelectrics, pyroelectrics and piezoelectrics.

1.2.1 Landau theory for ferroelectric:

A ferroelectric is an insulating system with two or more discrete stable or metastable states of different non-zero electric polarization in zero applied electric field It is also called as "spontaneous" polarization.[5] LT is particularly well-suited for those systems with long-range interactions i.e. superconductors and ferroelectrics. LT is a symmetry-based analysis of equilibrium behavior near a phase transition. Landau theory is a macroscopic approach and thus it cannot

describe any microscopic physics viz. atomic displacements etc. associated with the phase transition.[6]

A ferroelectric crystal mostly has certain regions which exhibit a uniform alignment of electric dipoles and the spontaneous polarization in such regions may be different from one another. Such regions with uniform polarization are called ferroelectric domains. The interface between two domains is called the domain wall.

The most important property of ferroelectric materials is the formation of hysteresis loop due to its polarization reversal property. Figure 1.3 shows the ferroelectric hysteresis loop of ferroelectric materials.

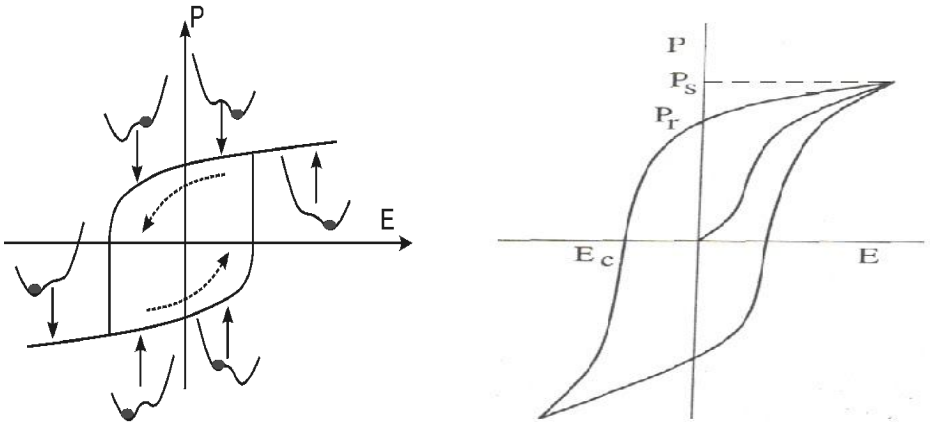

Figure 1.3: (a) Schematic picture of hysteresis in an idealized ferroelectric. (b) A typical P-E hysteresis loop of ferroelectric material.

Up to certain electric field the ferroelectric material shows the linear relationship between electric field (E) and polarization (P) and is called the dielectric ($P \propto E$). After that at relatively high electric field polarization, it shows a nonlinear relationship with the field as shown by ferroelectrics. Polarization gets saturated at a certain higher field called saturation polarization. When the applied field is removed the material still possesses some polarization as some domains do not come back to the original direction. This polarization is called remnant polarization. In order to remove the remnant polarization in the material, an extra amount of opposite electric field is required which is known as

coercive field. With an increasing electric field more domains will align in the opposite direction. Hence the cycle in fig. 1.3(b) shows it which is obtained by inverting the electric field once again.

The ferroelectricity phenomenon was first observed in Rochelle salt [7].Multi-ferroic materials are those systems which has the co-existence of any two or more ferroic order parameters, i.e., they can have simultaneous existence of ferro-electricity (ordered electric dipole moments) or ferro/ferri/antiferro-magnetism (ordered magnetic moments) or ferroelasticity (ordered strain arrangements). Most of the multiferric materials are based on perovskite transition metal oxides, rare-earth mangnaites & ferrites such as $HoMn_2O_5$, $LuFe_2O_4$, $BiFeO_3$, $HoMnO_3$, $BiMnO_3$ etc. However, most of these systems exhibit multiferroism well below the room temperature.

1.3 Magnetism:

Magnetite or lodestone (FeIIOFeIII2O3) mineral in its natural state often has a strong attraction for iron and steel find in magnesia First magnetic technological invention -compass: in China, sometime between 2500 B.C. Early theories and experiments on magnetism were developed by the great minds of all times -Gilbert, Descartes, Coulomb, Poisson, Green, Oertsted, Ampere, Davy, Freesnel, Faraday,Maxwell etc. Magnetism is a class of physical phenomena that includes forces exerted by magnets on other magnets. All magnetic materials respond to an external magnetic field (H). The magnetization (M) of a sample is proportional to H:

$M = \chi H$. The proportionality constant, χ, is the magnetic susceptibility. The primary magnetic field B is related to the magnetic field H and magnetization by $B= \mu(H+M)$. The sources of magnetic field are electric current and magnetized material. We begin with magnetostatics, the classical physics of the magnetic fields, force and energies associated with distribution of magnetic material and study electric current. The concepts presented here underpin the magnetism of solids. The elementary quantity in solid-state magnetism is the magnetic moment m. On an atomic scale, intrinsic magnetic moments are associated with spin of

each electron and a further contribution is associated with its orbital motion around nucleus.[7]

1.3 Perovskites structure:

Perovskites gets its name from the Russian mineralogist L.A. Perovskii who saw these structures in the mineral $CaTiO_3$. The general chemical formula of perovskite is ABO_3 or a slighted distorted version where A and B are cations. The term complex in this context refers to structures where the A and/or B cation positions are occupied by more than one type of cation. A ions generally have a large ionic radius (Pb^{2+} ,Ba^{2+} ,Ca2+ …..) and B ions (Ti4+ ,Mg2+…..) mostly have a small ionic radius. The ideal perovskite structure has a cubic unit cell of the side about 3.9Å, space group Pm3m and it contains one formula unit. The B ions have an octahedral oxygen coordination and the A ions have 12 fold coordination. The oxygen ions having six cation (4A+2B). There are many ABO_3 compounds for which the ideal cubic structure is distorted to a lower symmetry (e.g. tetragonal, orthorhombic, etc.).

The valency of the A cation ranges from +1 to +3 and the B cation from +3 to +6. The 'A' atoms are larger than the 'B' atoms. The perovskite structure consists of corner shared oxygen octahedral with B site cation in the middle. The A cations are situated at interstitial sites created by oxygen octahedral.

The unit cell of perovskite structure can be distorted in many different directions viz. [100], [110], [111], [hkl] accompanied by the tilting of oxygen octahedra. In the ideal perovskite structure ,where the atoms are touching each other, the B-O distance is equal to a/2 and the A-O distance $\sqrt{2}(a/2)$(a is the cubic unit cell length).[8]

1.3.1 Tolerance factors in perovskites:

Goldschmidt introduced “tolerance factor” which tells us the distortion form of an ideal cubic structure.

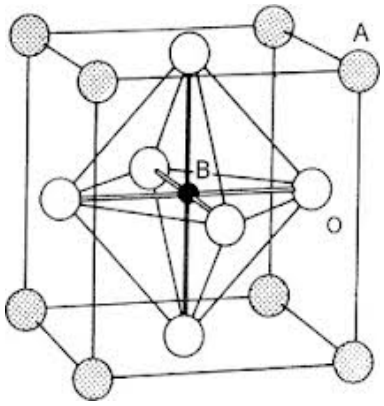

Fig 1.4 Perovskite structure.

$t=(<r_A>+r_O)/\sqrt{2}(<r_B>+r_O)$

Here, r_A, r_B and r_O are the radii of A, B and O ions.$0.75<t<1.05$ for most of the material. If B radius are small,the oxygen octahedra are unstable due to oxygen-oxygen ionic repulsion and $rA<\sqrt{2}(ro+Rb)/ro$ is adjusted by rotations of oxygen octahedral.

1.3.2 Perovskite structure of NBT

$Na_{0.5}Bi_{0.5}TiO_3$ (NBT) is one among the promising lead free ferro/piezoelectric material discovered by Smolensky et. al., in1960s. NBT contains bismuth (Bi^{3+}) and sodium (Na^{+}) cations which occupy the corners of a cubic unit cell, oxygen (O^{-2}) cations occupies the face centers forming an octahedral while the titanium (Ti^{4+}) cation occupies the center of the oxygen octahedral site exhibiting a rhombohedral structure with *R3c* symmetry at room temperature.

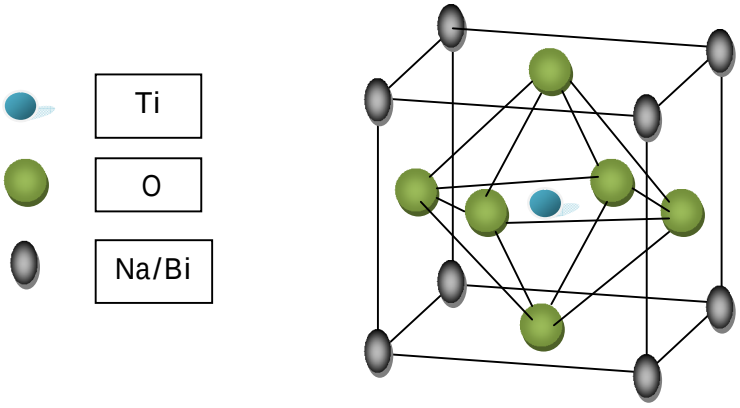

Fig 1.5 Perovskite structure of NBT

With decreasing temperature, NBT transforms from cubic Pm3m to tetragonal P4bm and rhombohedral R3c with coexistence regions between them.

1.4 NBT and related material

The excellent ferroelectric and piezoelectric properties of lead based ferroelectric materials are shown. These materials contain a large amount of lead which is toxic. While processing these materials, lead (Pb) is released into the environment. The restoring of the lead-based materials has extensive environmental issues. Since lead remains for a long time in the environment and accumulates in living tissues, it damages the brain and nervous system [9].

There are various lead free perovskite ferroelctric materials e.g., $BaTiO_3$ (BT), $Na_{0.5}Bi_{0.5}TiO_3$ (NBT), $K_{0.5}Bi_{0.5}TiO_3$ (KBT), $KNbO_3$ (KN), $K_{0.5}Na_{0.5}NbO_3$ (KNN), $BaZrTiO_3$ (BZT), $BaSrTiO_3$ (BST) and their solid solutions have been studied for lead free applications [9]. Among the lead free ferroelectric materials, $Na_{0.5}Bi_{0.5}TiO_3$ (NBT) is considered to be an excellent candidate for applications.

Sodium bismuth titanate ($Na_{0.5}Bi_{0.5}TiO_3$), NBT and NBT-based materials show excellent properties and are considered to be an excellent candidate as a key material for lead-free piezoelectric materials. NBT has a rhombohedral perovskite-like structure with Na^+ and Bi^{3+} ions randomly distributed at the 12-fold octahedral sites. NBT have a large remanent polarization of P_r =38 $\mu C/cm^2$ at room temperature. However, because of its high coercive field

(E_c=7.3kV/mm) the poling of NBT becomes very difficult. NBT also exhibits several interesting high temperature structural phase transitions. Hence it will be an interesting study to induce multiferroism in such systems.

There are some important features of the NBT material given below:-

1. NBT has the special ability to form a stable chemical compound through substitution on the A-site cation in the perovskite structure [10].
2. Many relaxor ferroelectrics have pairs of isovalent A cations or chemically different B cations, but NBT has unlike valency Na^+ and Bi^{3+} cations at the A sites.

Studies on the structural and electrical properties have been performed on NBT and its dopants. Some of them improve the dielectric properties, while others try to improve the piezoelectric properties. NBT is a good material for both applications because it can be modified to enhance a specific desirable behavior. The complex substitutions of Ba^{2+}, Sr^{2+} and Mn^{4+} cations reduces coercive field and increases the polarization of NBT and this was explained using the first principle derived approach [11]. Recently K.,B. et al. [12] observed a diffuse phase transition study on $Ba2^+$ substituted NBT ferroelectric ceramic. NBT has rhombohedral symmetry at room temperature ,it undergoes a series of phase transition (1) ferroelectric rhombohedral to antiferroelectric tetragonal around 230^0C, (2) antiferroelectric tetragonal to non-polar tetragonal around 320^0C, (3) cubic to tetragonal symmetry takes place in the temperature range of 520-540^0C. Some researchers investigated the effect of small amount of dopants viz. Fe, Mn, Ni on dielectric and piezoelectric properties for perovskite ceramics.[13]

Interestingly, experimental results have demonstrated the presence of the ferromagnetic order in Fe, Mn, and Co-doped $BaTiO_3$ single crystals, ceramics, thin films, nanoparticles, and multilayers. More recently, Liu et al. [14] observed paramagnetism in Co,Cr, Fe-doped $BaTiO_3$ nanoparticles. Similarly Mn-doped $SrTiO_3$ also claims to exhibit rather different and complex magnetic ordering below 40 K, associated with magnetoelectric coupling. But in the recent study

conducted by Matjaz Valant et al it was found that there was no magnetic order. Therefore no magnetoelectric coupling exists in the bulk Mn-doped $SrTiO_3$ system. Hence, the observed magnetic properties result from external sources. However they suggested that processing conditions also play major role in determining the intrinsic magnetic behaviour of such systems.[15]

These inconsistent results and reports prove that the origin and nature of ferromagnetism in ABO_3 based ferroelectric materials are still a topical issue, similar to the case of dilute magnetic semiconductors. In this context we have chosen NBT as system to induce multiferroic behaviour by site specific cation substitution at Ti-site and also through different processing conditions.

Chapter 2

Experimental Technique

2.1 Introduction:

Ceramic processing is a sequence of operations that systematically changes the chemical composition and physical aspects of the structure which ultimately effects the physical properties of the material. The aim of the science behind ceramic processing is to identify the important properties and to understand the effect of processing parameters on the structural and physical properties of the materials. Ferroelectric ceramic materials can be synthesized in two forms i.e., single crystal and powder form.[16]

2.2 Various types of synthesis technique:

Ceramic powder synthesis is the most important technology in chemical engineering and ceramics related areas of materials science. The basic idea is that synthesis technique should give uniformity in the microstructure of a single phase ceramic for better properties. There are mainly two method for synthesis of ceramic powder. One is the chemical method and the other one is the mechanical method. Mechanical methods are (a) solid state reaction process and (b) high energy ball milling (ball mill, planetary ball mill, rotator ball mill, etc.). The chemical methods of synthesis of ceramic powders are sol-gel methods. But here we are using only solid state reaction process that I will discuss below.[17]

2.3 Equipment used:

Agate mortar & pestle, digital weighing balance, hot air oven, powder x-ray diffractometer (PANalytical Xpert pro), vibrating sample magnetometer (VSM),

2.4 Solid state reaction route:

The solid state reaction route is the most convenient and widely used method for the preparation of polycrystalline solids from a mixture of solid. Mostly solids do not participate in reaction at room temperature.

2.5 Reagents:

Reagents are the raw materials for the reaction from which the required solid crystalline compound will form as product. The nature of raw material has a major effect on the properties of the final ceramic material. The quality of raw materials depends upon the purity percentage. The reagents are selected on the basis of reaction conditions and the nature of the product.

2.6 Calcination:

Calcination is a thermal treatment process for solid materials in order to bring about thermal decomposition, phase transition, or removal of a volatile fraction. The heating of the mixture depends on the form and reactivity of the reactants.

2.7 Sintering:

Sintering was studied fundamentally and scientifically after 1940's. Sintering is a processing technique that is used to produce density-controlled materials, powder-metallurgical parts and bulk ceramic components by applying thermal energy. In general sintering processes can be divided into two types: solid state sintering and liquid phase sintering. Solid state sintering occurs when the powder compact is densified completely in a solid state at the sintering temperature (below the melting point). In the sintering process we can improve the strength of the material. Proper furnace control is important for optimum properties. Three stages are distinguished in sintering process. (a) first stage (initial), (b) second stage (intermediate), (c) third stage (final)

.

2.7.1. First stage (initial):

After burn out of any organic additives, two things happen to the powder particles when the mobility of the surface atoms has become high enough; initially rough surface of the particles is smoothed and neck formation occurs. The initial stage is characterized by the formation of necks between particles and its contribution to compact shrinkage is limited to 2–3% at most. We can used the two-particle model for the initial stage. Figure (2.1) shows two geometrical models for two spherical particles: one without shrinkage (a) and the other with shrinkage (b). In Figure (a), the distance between the particles does not change but the neck size increases as the sintering time increases.

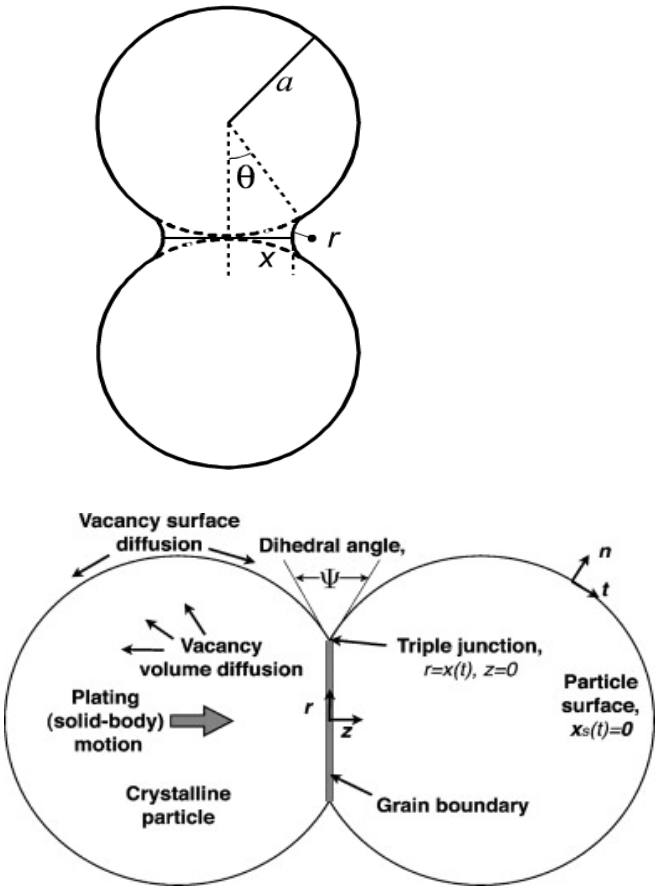

Fig.2.1 (a) without shrinkage and (b) with shrinkage

If the dihedral angle (ψ) between the particles is 180^0 and the grain size does not change during sintering, the radius of neck curvature r, neck area A and neck volume V are respectively. Without shrinkage (a)

$$V=\pi x^4/2a \qquad \ldots(2.1)$$

With shrinkage (b)

$$V=\pi x^4/4a \qquad \ldots(2.2)$$

2.7.2. Second stage (intermediate):

If grain boundaries are formed after the first stage, they form the new source of atoms for filling up the concave areas which diminishes the outer surface of the particle. During the intermediate stage, considerable densification, up to 93% of the relative density, occurs before isolation of the pores. We can use the channel pore model for the intermediate stage.

2.7.3. Third stage (final):

After second stage grain growth takes place, the pores break up and form closed spherical bubbles. The final stage involves densification from the isolated pore state to the final densification. We used the isolated pore model for the final stage.

2.7.4. Sintering mechanism:

- Six distinct mechanisms can contribute to the sintering of a consolidated mass of crystalline particles
  - Surface diffusion
  - Lattice diffusion from the surface
  - Vapor transport

- Lattice diffusion from the grain boundary
- Grain boundary diffusion
- Plastic flow[18,19]

2.7.4.1 Surface diffusion:

Diffusion is the most important sintering mechanism. The diffusion mechanism is related to the movement of atoms under a difference in vacancy concentration. Atom movement itself may be interpreted physically in two ways: first atom movement as a result of vacancy diffusion due to a difference in vacancy concentration and the second being the movement of the atoms themselves under a difference in stress. Surface diffusion initiates at low temperature in compression with other sintering mechanism.

2.7.4.2 Lattice diffusion from the surface:

Sintering by surface diffusion occurs via atom movement on the surface of the spheres from the sphere surface to the neck surface. In this case a stress gradient derived from the capillary pressure on the neck surface may be assumed to be present up to the region within a distance equal to the neck curvature radius. This means that there is no stress gradient beyond a distance equal to the neck curvature radius and that the neck growth is controlled by atom transport by surface diffusion from this region.

2.7.4.3 Vapour transport:

The driving force behind vapour transport is the energetically favorable reduction of surface area. This reduction is achieved due to the differential partial pressures over curved surfaces causing a mass flow from grains to necks, as well as from smaller to larger grains.

2.7.4.4 Lattice diffusion from the grain boundary:

The lattice diffusion of atoms from the grain boundary to the neck allows the boundary to act as a site for vacancy annihilation. The idea of atom movement

from a grain boundary under compressive stresses to another grain boundary under tensile stresses during creep is the same as that of vacancy movement in the reverse direction. If lattice diffusion of atoms from the grain boundary to the neck surface is to occur, the neck region must be under tensile stresses and the grain boundary under compressive stresses. In this regard it would be reasonable to consider that a stress gradient is present along the grain boundary from the neck center to the neck surface, as calculated by Exner and Bross. By this sintering mechanism, not only neck growth occurs but also a center-to-center approach of the two particles, i.e. shrinkage, takes place because material is removed from the contact area of the particles.

2.7.4.5 Grain boundary diffusion:

Grain boundary diffusion is relatively important to the sintering densification of most metal and many compounds. As sintering progresses, transport take place between pores via the grain boundary, leading to pore coarsening. Vacancy accumulations on a grain boundary require motion of the boundary, and this is resisted by contacting neighbor. It is the high grain boundary energy that is a prime cause of simultaneous grain growth during sintering (to add a species Ni, Mn, Co, Fe etc.)

2.7.4.6 Plastic flow:

Plastic flow is the motion of dislocation under stress. Dislocation participates in sintering during heating. Demonstrated densification rate improvement because of dislocation climb with the rate of pore elimination.

2.8. Electroding:

The sample surfaces were polished for smoothness and then silver paint is used as an electrode. The material is now in between two electrodes like dielectric material in between parallel plate capacitor. The electrodes also can be made by a deposition method using sputtering. Here we use the VSM (vibrating sample magnetometer).

2.9 Experimental Details:

The materials were synthesized by a conventional solid-state reaction route. The high purity (99.99%) sodium carbonate (Na_2CO_3), and oxides (Bi_2O_3, TiO_2, CoO_2) of required precursors were weighed according to the particular stoichiometric ratios according mole % calculation. The above weighed powder was mixed by agate mortar and pestle for 3 hours with synthesis acetone (CH_3COCH_3) medium till it dry for homogeneous mixture. The dried mixture was put in alumina crucible and calcined at temperature 800 ^{0}C for 3 hours in air circulate furnace. The above heated powder was formed into a piece and it was grinded till it became fine powder. The calcined powder was grinded for fine powder and phase formation was checked by XRD at room temperature. The calcined powder was put in RETSCH Planetary ball mills in grinding jar for 5 hours. The ball milled sample formed into a powder after grinding. The ball milled powder was mixed with PVA (polyvinyl alcohol) as a binder. The binder mixed powder was compacted to form pellet b**y** . The sintering of the pellet sample was carried out at an optimized temperature of 1150 ^{0}C in presence of O_2 (oxygen) for 3 hours for densification. The sintered pellets were polished by carbon paper and painted with silver paste as an electrode for electrical measurement.

2.10 FLOW CHART

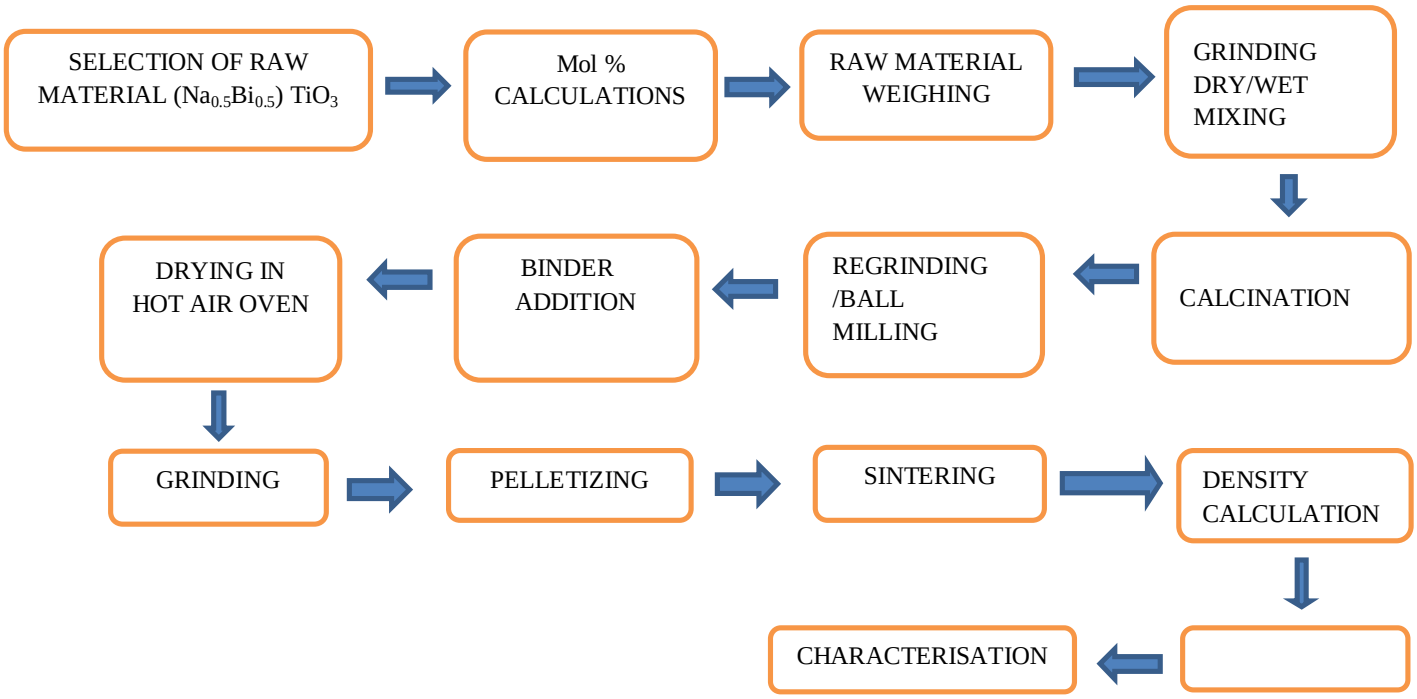

Fig 2.3 Flow chart for the preparation of ceramic samples by a solid-state reaction technique.

2.11 Characterization Techniques:

The synthesized materials are characterized by various experimental techniques at different measurement conditions to study its physical properties. The basic fundamental principle and use of XRD, SEM, and VSM, study are described below.

2.11.1 XRD (X-ray diffraction) :

X-rays were discovered in 1895 by the German physicist Roentgen. X-ray 9diffraction (XRD) characterization technique is a useful for detailed structural study of the material. It gives information about determination of the

crystal structure, atomic arrangements of materials, phase ,measurement of particle size, determination of the orientation of the crystal and identification of the chemical species present in materials which are the origin of physical properties.[20,21]

This was recognized by Max von Laue in 1912 who, by his theoretical work, laid the foundations for X-ray diffraction as the principal technique for structure determination. To interpret interference patterns formed by diffraction, lattice planes can be regarded as a stack of plane with spacing d_{hkl} that reflects the incident radiation (Figure 2.2).

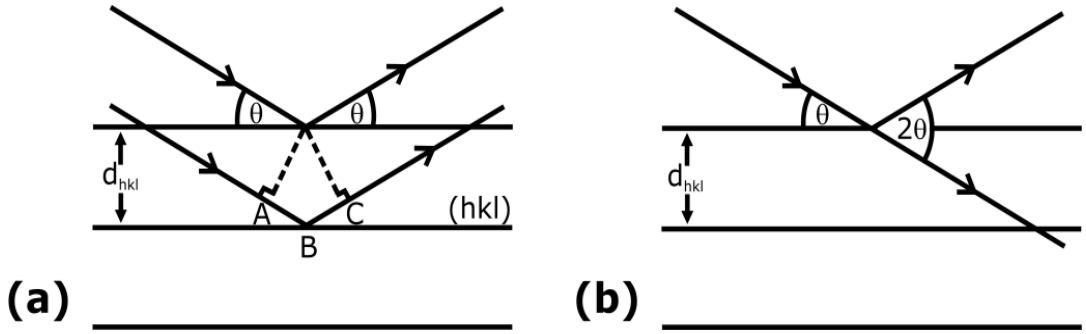

Figure 2.2: Graphic representation of the Bragg condition: (a) path difference between X-ray "reflected" from successive planes; (b) X-rays incident on a set of planes at Bragg angle θ are diffracted through an angle 2θ (after Putnis 1992).

The portion of the beam that passes the first "plane" unscattered may interact with the second or third layer of atoms and so on. The correlation between wavelength, λ, Bragg angle, θ, and lattice plane spacing, d_{hkl}, is given by the

$$n\lambda = 2d_{hkl}\sin\theta \qquad \text{(Bragg equation)} \qquad \ldots 2.3$$

Where n is the order of diffraction. For n=0, we get zeroth order reflection which occurs for θ =0 viz., in the direction of the incident beam and hence it cannot be observed experimentally, so often we are using the diffraction lines appearing for n=1,2 and 3 are called first, second and third order diffraction lines respectively and so on.

Constructive interference occurs if the path difference between reflections from adjacent planes is equal to an integral multiple, n, of λ. For monochromatic

X-radiation (λ = const.), constructive interference takes place at certain Bragg angles. For the identification of crystalline phases, the Bragg angles measured are used to calculate lattice plane spacing which are then compared to data sets of well-defined structures. In the original experimental setup of von Laue, polychromatic X-rays were collimated onto a single crystal, as certain wavelengths would fulfill the Bragg condition without requiring an exact orientation of the sample. An alternative method using monochromatic radiation was soon developed by Peter Debye, Paul Scherrer and, independently, Albert Hull. By preparing powder samples, they found a simple way of obtaining crystallites with statistical orientation. For example, a fraction of the crystallites will be oriented in such a way that their (1 1 1) planes with spacing d_{111} produces a reflection at glancing angle $2\theta_{111}$. Due to the random angular orientation around the incident beam axis, the reflections are confined to the surface of a cone with aperture semi-angle 2θ (Figure 2.3). As other crystallites contained in the sample meet the Bragg condition for different d_{hkl} values, they will produce reflections corresponding to a set of cones whose positions and intensities are recorded as the diffractogram.

Powder XRD is a standard technique for phase identification and the determination of lattice parameters for single phases and mixtures. X-ray diffraction experiments were performed on a PANalytical X'Pert-Pro diffractometer in a wide range of Bragg angle ($20<2\theta<80^0$) with CuKα-radiation (1.54187 Å) [Cu Kα_1-radiation (1.54059 Å); Kα_2-radiation (1.54442 Å)] at a continuous scan type having a step size of 0.0167° degree at room temperature. and 40 kV acceleration voltage. Interaction of the electrons with the anode material causes the emission of a continuous X-ray spectrum superimposed by characteristic lines of the target.

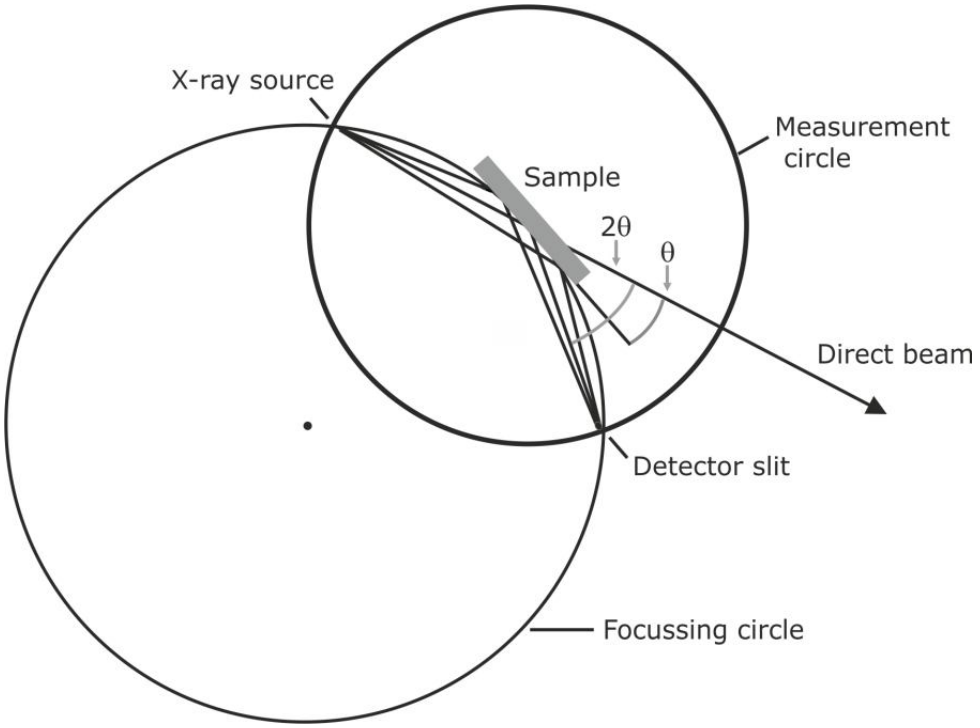

Fig 2.3 Geometry for X-ray powder diffraction

During measurement, continuous rotation of the sample around its axis increases the number of particles contributing to the diffraction pattern.[22]

2.11.2 VIBRATING SAMPLE MAGNETOMETER:

2.11.2.1 Introduction:

Foner (1956) was the first to describe a VSM for the measurement of magnetic moments, his design has become generic to all subsequent designs.[23] The VSM comprises two principle components, the sample vibrator mechanism and the induction signal detection coils, the latter being situated in close proximity to the sample which is also positioned in an external magnetic field. It is required that the sample vibrates in a periodic and stable manner.

In VSM methods of measuring magnetic moments can be divided into three parts; first measurement of a force on a material in a non-uniform magnetic field, second measurement of magnetic induction in the vicinity of the sample, and

third indirect measurements of phenomena which tells us the magnetic properties. The indirect techniques for measuring magnetic moments include measurement of the Faraday effect. The general problem of indirect techniques is that they are limited to particular phenomena which are observable in a limited class of materials about which considerable prior knowledge is required. A particularly successful vibrating-coil technique has been developed by D. O. Smith. The novel features of this magnetometer are: first, sample motion perpendicular to the applied field; and second, detection coil configurations, with effective area-turns non-symmetncally distributed about the axis of vibrations, which permit this oscillating dipole field to be observed.[24]

2.11.2.2 Principle:

A VSM operates on Faraday's law of induction. According to Faraday's experiments, a static magnetic field produces no current flow, but a time-varying field produces an induced voltage (efm electromotive force) in a closed circuit, which causes a flow of current. Faraday discovered that the induced emf. V_{efm} (in volts), in any closed circuit is equal to the time rate of change of the magnetic flux linkage by the circuit. This is called Faraday's law, and it can be expressed as

$$V_{efm}=-d\lambda/dt=-N\, d\varphi/dt \qquad \text{.....(7.2)}$$

Where N is the number of turns in the circuit and φ is the flux through each turn. The negative sign shows that the induced voltage acts in such a way as to oppose the flux producing it. [25] Faraday's law of induction, which tells us that a changing magnetic field will produce an electric field. This electric field can be measured and can tell us information about the changing magnetic field. A VSM is used to measure the magnetic behavior of magnetic materials.

A VSM operates by first placing the sample to be studied in a constant magnetic field. If the sample is magnetic, this constant magnetic field will magnetize the sample by aligning the individual magnetic spins, or the magnetic domains, with the field. A vibrating-sample magnetometer, measures the magnetic moment of a sample when it is vibrated perpendicularly to a uniform

magnetizing field called the magnetic stray field. When the sample is moved up and down, this magnetic stray field changes as a function of time and can be sensed by a set of pick-up coils. The alternating magnetic field will cause an electric field in the pick-up coils according to Faraday's Law of Induction. This current will be proportional to the magnetization of the sample.

The induction current is amplified by a trans-impedance amplifier and lock-in amplifier. We are using the Model P525 Vibrating Sample Magnetometer (VSM) measurement system for the Physical Property Measurement System (PPMS) is a fast, sensitive and fully automated DC magnetometer. PPMS system properties Temperature range: 1.9 K - 400 K, Magnetic field: up to16 tesla, Magnetic field ramp rate: determined by magnet and power supply, Temperature and magnetic field may be ramped during the measurement. The various components are hooked up to a computer interface but the P525 VSM requires a PPMS computer system running Microsoft Windows^{XP} software. Using controlling and monitoring software, the system can tells us how much the sample is magnetized and how its magnetization depends on the strength of the constant magnetic field.

2.12 PES (Piezoelectric Evaluation System):

Electrical measurement method:- Electrical and electromechanical characterization of piezoelectric materials are the decisive factor to investigate their suitability for piezoelectric or pyroelectric sensor and actuator devices. For the electrical characterization of a sample is the measurement of its current due to an applied electrical excitation voltage and the electromechanical characterization measuring the samples mechanical displacement or by applying a mechanical strain and recording the resulting charge displacement. The total polarization charge is determined by the geometry of the capacitor, the material and the applied voltage. The charge in voltage per time, which is called slew rate. The magnitude of the current flow during a polarization reversal in a ferroelectric capacitor can be calculated as

$Q=D.A$

$Q=P.A$

$I=dQ/dt=A(dP/dV)(dV/dt)$

Where I is magnitude of the current, Q is charge, A is area of the capacitor, P the polarization of the material, V the applied voltage, dV/dt is the slew rate of the signal from that is applied.

There are three established method to record the charge and current response of the sample.

1. Sawyer tower method:- It is based on a charge measurement method keep on a reference capacitor in series with the ferroelectric capacitor (V=Q/C). This method can be used up to a high speeds which is basically limited by cable reflection. Typical cable capacitance values are between 33pF and 100pF per meter. Moreover the input resistance of the voltage measurement device in parallel to the reference capacitor. This method is less suitable foe slow measurements because this loads to a discharge with a corresponding time constant.
2. Shunt method:- This measurement method is based on a current method viz. the switching is measured as a voltage drop at the shunt resistor (V=R*I). In this method also get similar kind of difficulties as in case of the ST method. But in this case the cable capacitance for the voltage measuring device in parallel to the reference resistor.
3. Virtual ground method:-This method uses a current to voltage converter which is based on current measurement using an operational amplifier with feedback resistor. This method is helpful for measurement especially of small capacitor as the cable capacitance is physically in place but electrically ineffective, because both electrodes of the capacitor are kept on same potential and sample is always applied to the full excitation voltage, since there is no back voltage. VG method enables the highest precision for

ferroelectric measurements. Therefore it is used as integral part of axiACCT measurement system.

Fig. 2.4 shows the equivalent circuit of the VGM.

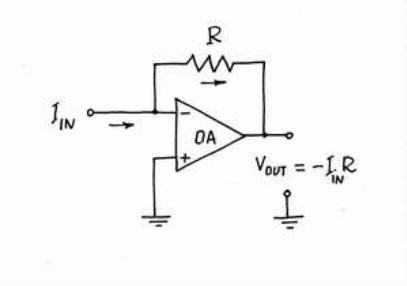

Fig 2.4 VGM

Chapter 3

Results and Discussion

3.1. X-Ray Diffraction analysis:

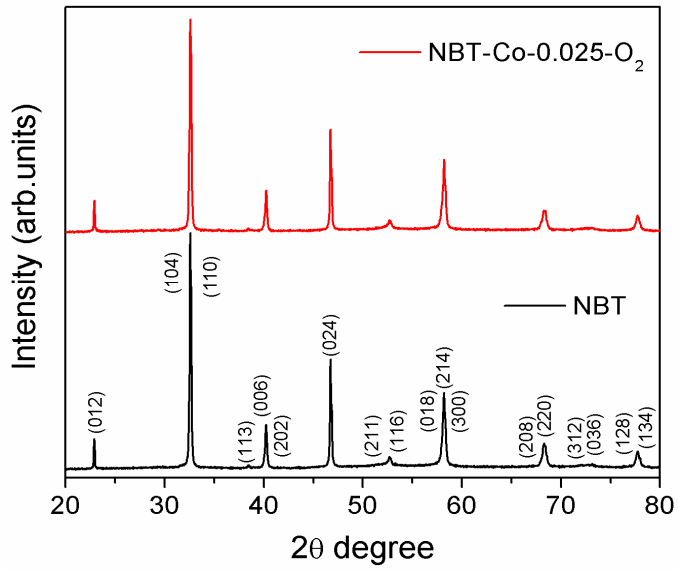

Fig.3.1. XRD pattern for NBT and NBT-Co sample measured at room temperature

X-ray diffraction experiments were performed on a PANalytical X'Pert-Pro diffractometer in a wide range of Bragg angle ($20<2\theta<80^0$) with CuKα-radiation (1.54187 Å) [Cu $K\alpha_1$-radiation (1.54059 Å); $K\alpha_2$-radiation (1.54442 Å)] at a continuous scan type having a step size of 0.0167° degree at room temperature. The XRD pattern of the sintered $Na_{0.5}Bi_{0.5}TiO_3$ (NBT) and $(Na_{0.5}Bi_{0.5})Ti_{0.975}Co_{0.025}O_{3\pm\delta}$ (NBT-Co) at room temperature is shown in Fig. 3.1. All the Bragg peaks of NBT sample matched well with the JCPDS file. no: 360340 (JCPDS-Joint Committee on Powder Diffraction Standards) which belong to rhombohedral structure and *R3c* space group. Similarly the NBT-Co sample also reflects a similar kind of Bragg peaks with other secondary phases being observed. This confirms that NBT-Co sample also crystallizes in *R3c* Space group. In order to see the effect of Co-ion substitution some of the major Bragg peaks of both NBT and NBT-Co samples were scanned slowly with same scanning rate. Fig. 2(a) - 2(d) shows the enlarged view of slow scanned Bragg

peaks in the range from 22.7° - 23.1°, 32.2° -33°, 46.2°- 47.2° and 37.5° - 41.5° respectively. It was observed from Fig. 2(a) - 2(d) that there is no significant change in the (012) and (024) Bragg reflections for NBT-Co sample when compared with the NBT. However there was some change in the NBT-Co sample in the (110) and (202) Bragg reflections with a higher degree shift in the 2θ position. This indicates that there is some decrease in the d-spacing in the NBT-Co sample due to Co-ion substitution.

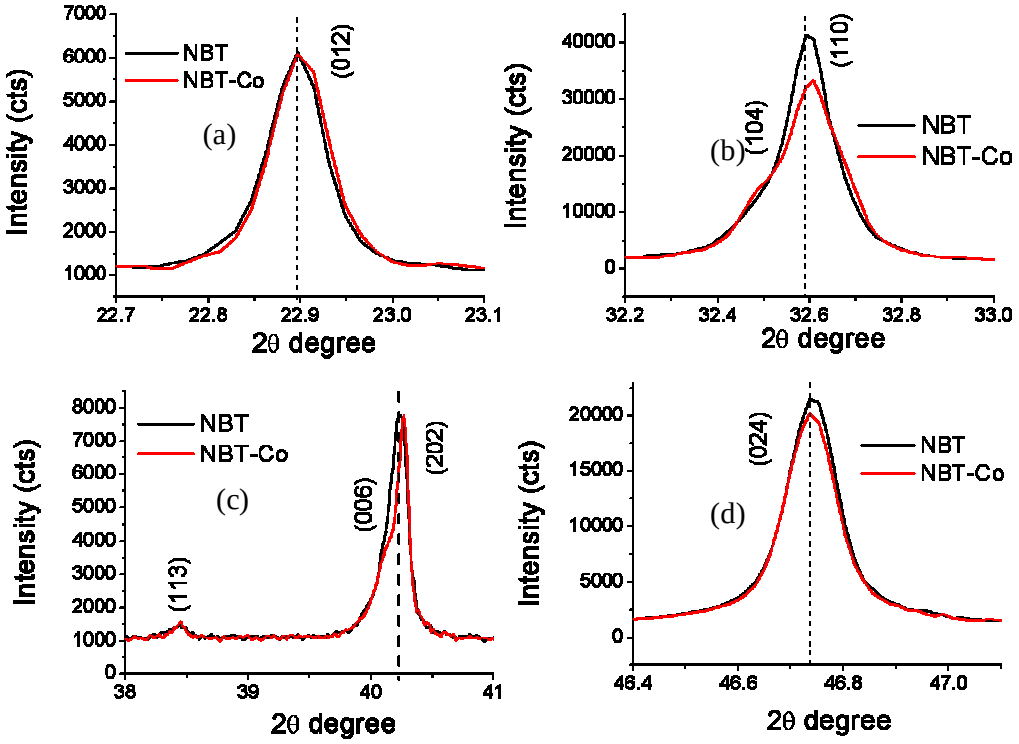

Fig.3.2. XRD pattern showing the enlarged view of certain Bragg reflections corresponding to NBT and NBT-Co samples at room temperature.

In order to see the exact change in the NBT host lattice due to Co-ion substitution we have calculated the lattice constants of both NBT and NBT-Co sample using Least Square fitting software. Lattice parameters are calculated using a hexagonal frame of reference and it is shown in the Table 3.1. It is evident from the lattice parameters that there is an increase in the c/a ratio and a slight decrease in the unit cell volume for NBT-Co sample. This indicates that there is possibility of mixed valence states of Co-ions persist in the NBT-Co

sample, which is also evident from the Shannon ionic-radii as shown in Table.3.2. To have an insight about the possibility of mixed valence states, we have calculated the tolerance factor t, by considering the individual valence states of Co^{2+} (High spin), Co^{3+} (High spin) and Co^{4+} (High spin) at Ti-site with their corresponding composition as shown in the Table 3.3. However, it was found that there is an increase in the t-factor if we consider only the individual valence states. This further gave an insight that there is a possibility of mixed valence state. Hence in order to match the tolerance factor close to NBT, a mixed valence states of Co-ion were carried out by certain permutations and combinations as shown in Table. 3.4. Even though it doesn't match close to that of NBT.

Table: 3.1. Lattice constants of NBT and NBT-Co sample

Composition	Lattice parameter a_{hex} (Å)	Lattice parameter b_{hex} (Å)	c/a ratio	Volume ($Å^3$)
$(Na_{0.5}Bi_{0.5})TiO_3$	5.48566	13.47586	2.4565	351.1726
$(Na_{0.5}Bi_{0.5})Ti_{0.975}Co_{0.025}O_{3\pm\delta}$	5.48068	13.50034	2.4632	351.1710

Table. 3.2. Shannon ionic radii corresponding to their possible valence and spin state of six coordinated (6-CN) Cobalt octahedral complex ion.

Valence State	$3d^n$-configuration	C.N	Spin state	Ionic radii r (Å)
Ti^{+4}	3d 0	6	-	0.605
Co^{+2}	3d 7	6	LS	0.65
Co^{+2}	3d 7	6	HS	0.745
Co^{+3}	3d 6	6	LS	0.545
Co^{+3}	3d 6	6	HS	0.61
Co^{+4}	3d 5	6	HS	0.53
HS= High spin; LS= Low spin				

Table. 3.3. Tolerance factor calculation by considering individual spin state of Co-ion

Valence state	Composition	Tolerance factor (t)
Ti^{4+}	$(Na_{0.5}Bi_{0.5})TiO_3$	0.9787
Co^{2+}(HS)	$(Na_{0.5}Bi_{0.5})Ti_{0.975}Co_{0.025}O_{2.975}$	0.9819
Co^{3+}(HS)	$(Na_{0.5}Bi_{0.5})Ti_{0.975}Co_{0.025}O_{2.975}$	0.9835
Co^{4+}(HS)	$(Na_{0.5}Bi_{0.5})Ti_{0.975}Co_{0.025}O_{2.975}$	0.9845

In the next attempt, a change in the oxygen stoichiometry was modified in order to match the t-factor, as we have performed the sintering under high oxygen partial pressure it is possible to have an increase in the oxygen stoichiometry. As seen in the Table 3.5 and 3.6, with the increasing the oxygen stoichiometry, the tolerance factor has reduced and it is almost close to NBT. Hence from these calculations, it is possible to have a qualitative idea that there is mixed valence state persist in the system along with a possible increase in oxygen stoichiometry due to the oxygen atmosphere sintering.

Table 3.4. Tolerance factor calculation by considering different permutation and combinations of Co-valence states for the composition $(Na_{0.5}Bi_{0.5})Ti_{0.975}Co_{0.025}O_{2.975}$

Ti^{4+}	Co^{2+}(HS)	Co^{3}(HS)	Co^{4+}(HS)	Ionic radii $<r_B>$(Å)	Tolerance factor (t)
0.975	0.005	0.0125	0.0075	0.605	0.9836
0.975	0.01	0.005	0.01	0.6058	0.9832
0.975	0.01	0.01	0.005	0.6062	0.9830

Table. 3.5. Tolerance factor calculation by considering different permutation and combinations of Co-valence states for the composition $(Na_{0.5}Bi_{0.5})Ti_{0.975}Co_{0.025}O_{2.990}$

Ti^{4+}	Co^{2+}(HS)	Co^{3+}(HS)	Co^{4+}(HS)	Ionic radii $<r_B>$(Å)	Tolerance factor (t)
0.975	0.005	0.0125	0.0075	0.605	0.9804
0.975	0.01	0.005	0.01	0.6058	0.9803
0.975	0.01	0.01	0.005	0.6062	0.9801

Table. 3.6. Tolerance factor calculation by considering different permutation and combinations of Co-valence states for the composition $(Na_{0.5}Bi_{0.5})Ti_{0.975}Co_{0.025}O_{2.995}$

Ti^{4+}	Co^{2+}(HS)	Co^{3+}(HS)	Co^{4+}(HS)	Ionic radii $<r_B>$(Å)	Tolerance factor (t)
0.975	0.005	0.0125	0.0075	0.605	0.9798
0.975	0.01	0.005	0.01	0.6058	0.9794
0.975	0.01	0.01	0.005	0.6062	0.9792

3.2 M-H curves:

Figure 3.3a shows the variation of momentum vs. temperature for a magnetic field, H = 250 Oe. This plot depicts the spin glass behavior. It could be observed that there is strong irreversibility between FC and ZFC and large bifurcation at low temperatures. ZFC and FC tend to the same value of moment at temperatures greater than 48 K. Figure 3.3b illustrates the variation of magnetic susceptibility (χ) and temperature for NBT Co. the tested specimen shows a very high susceptibility at a temperature of about 48K and then drops suddenly and tends to a constant value at temperatures higher than 48 K.

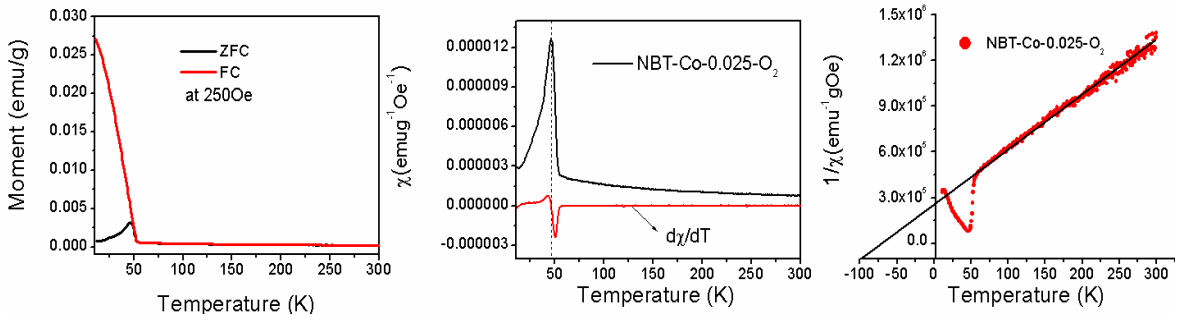

(a) (b) (c)

Fig 3.3 (a) Moment vs. temperature, (b) susceptibility vs. temperature, (c) Reciprocal susceptibility vs. temperature curves

Figure 3.3c shows the variation of reciprocal susceptibility vs. temperature. As expected, the reciprocal of magnetic susceptibility has a minimum value at 48 K and then increases. This indicates the presence of a second magnetic field.

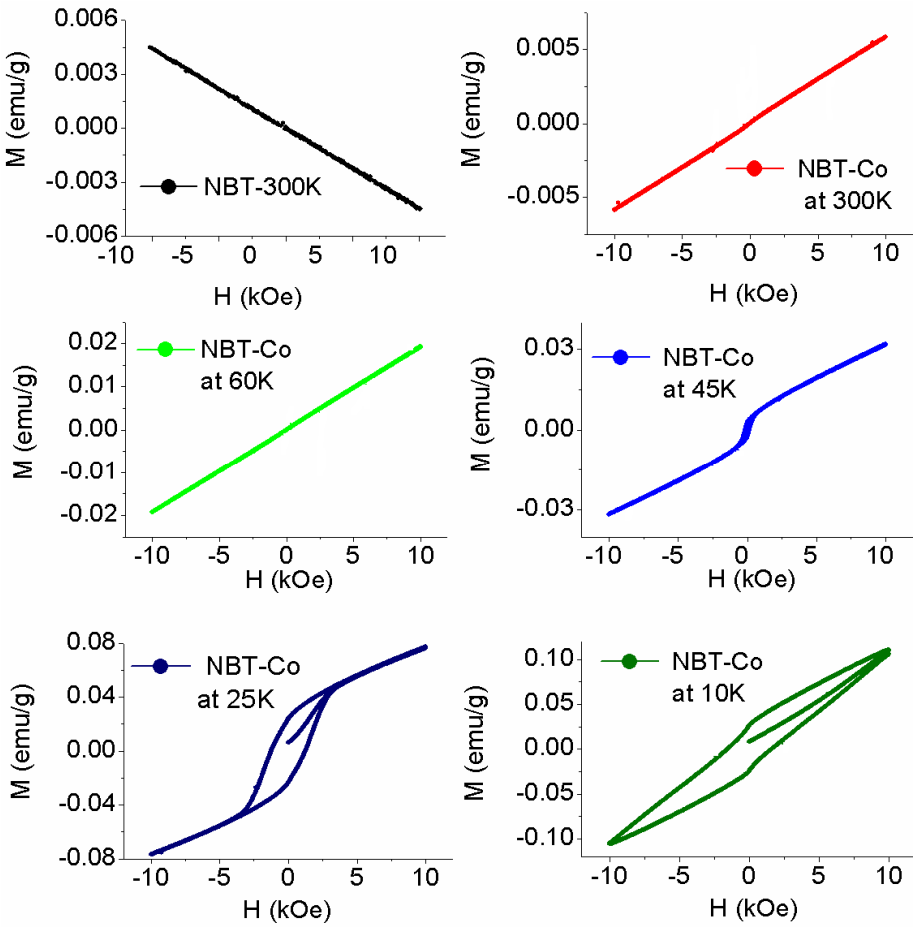

Fig 3.4 Magnetization vs. magnetic field NBT system diamagnetic, NBT-Co for different temperature peramagnetic, antiferromagnetic, weak ferromagnetic

Figure 3.4 illustrates the variation of magnetization vs. magnetic field at various temperatures. A decrease in magnetization could be observed with increase in magnetic field as depicted in Fig. 3.4a which indicates diamagnetic behavior for NBT tested at 300K. Figure 3.4b shows an increase in spontaneous magnetization with increase in magnetic field for a tested range of -10 to 10 kOe. This illustrates the paramagnetic behavior for NBT-Co at a temperature of 300 K. NBT-Co was tested at low temperatures of 60K and the paramagnetic behavior was observed (refer Fig. 3.4c). The specimen NBT-Co was tested at temperature of 45K and it deviated from paramagnetic behavior to a very small antiferromagnetic behavior (Fig. 3.4d). Fig 3.4e shows weak ferromagnetic behavior because at low temperatures the magnetic moment orientation changes. To understand the behavior

of the specimen at very low temperatures of 10K the specimen was tested and it showed the weakest ferromagnetic behavior.

3.3 P-E loop

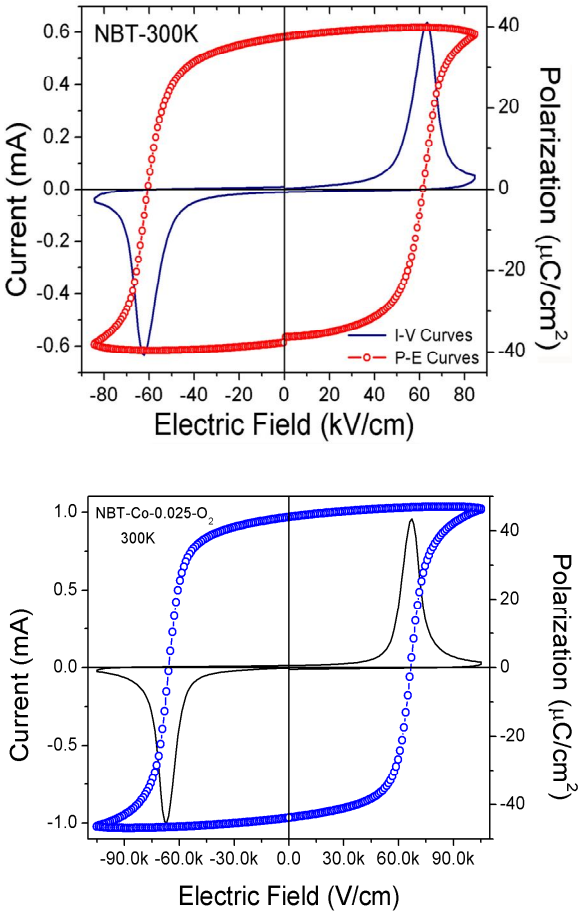

Fig 3.2 (a) The polarization versus electric field (*P–E*) and the displacement current versus electric field (*I–E*) of NBT (b)The polarization versus electric field (*P–E*) and the displacement current versus electric field (*I–E*) NBT -Co

The variation of current in mA vs. electric field in kV/cm and Polarization (μC/cm^2) vs. electric field for both NBT and NBT-Co was plotted at temperatures of 300K (Fig. 3.2). The pattern of ferroelectric hysteresis and loop formed for the variation of current vs. electric field remained the same for both NBT and NBT-Co. The ferroelectric hysteresis loop the remnant polarization and coercive field is different for the tested materials NBT and NBT-Co. NBT-Co has a remnant polarization of 43 μC/cm^2 compared to NBT which has 37 μC/cm^2 and hence NBT-Co could store more memory. As expected the coercive field of NBT-Co is lesser than NBT which helps in easy poling of NBT-Co.

3.4 Conclusions:

Polycrystalline $Na_{0.5}Bi_{0.5}Ti\ O_3$ and $Na_{0.5}Bi_{0.5}Ti_{0.975}\ Co_{0.025}\ O_{2.975}$ compounds were synthesized by conventional solid state route. All the compounds crystallize in the class of rhombohedral structure with R3c space group. In search of suitable lead free ferroelectric ceramics for the environmental concern, the structural and electrical properties of sodium bismuth titanate (NBT) and modified NBT have been investigated. The work contributes to the research and development of lead free perovskite ferroelectric material in the following aspects:

1 The samples were prepared using a high-temperature solid-state reaction route at an optimized calcination (800^0C) and sintering temperature (1100^0C) for NBT (air) and sintering temperature (1150^0C) for NBT - Co. (O_2).

2 The formations of the compounds were confirmed by XRD analysis.

3. M-H curves shows phase transition at different temperature. It was inferred from the study that at temperatures above 60K NBT-Co showed paramagnetic behavior and temperatures below 25K it shows very weak ferromagnetic behavior.

4. From P.E curved it could be observed that due to high remnant polarization characteristic of NBT-Co it could support the storage of high memory.

3.5 Future Work:

The study could be further improved by doping different transition metals like Zr, Fe, Mn etc. to NBT and the characteristic behavior could be studied.

Study of dielectric, piezoelectric and ferroelectric properties of thin films and single crystal of NBT based materials can be developed for application point of view

Dependence of grain size and other properties (piezoelectric, ferroelectric etc.) on sintering temperature can also be studied

The study of crystal structure at various temperature by temperature dependent X-ray diffraction from synchrotron radiation, neutron diffraction analysis and Raman spectroscopy can be performed.

References

[1] M. W. Barsoum, Fundamental of ceramics. Taylor and Francis. (2003)

[2] Elements of electromagnetics sadiku.

[3] Engineering Multiferroic Materials and New Functionalities in Material (2008) 1-13

[4] M. E. Lines and A. M. Glass, Principles and applications of ferroelectrics and related materials, Clarendon Press, Oxford (1977)

[5] K. Rabe, C. H. Ahn, J.-M. Triscone (Eds.): Physics of Ferroelectrics: A Modern Perspective, Top. Appl. Physics 105, (2007)

[6] P. Chandra and P.B. Littlewood A Landau Primer for Ferroelectrics (2008)

[7] Magnetism and magnetic materials J.M.D.Coey (22-40)

[8] J. Valasek, Piezoelectric and allied phenomena in Rochelle Salt. Physcial Review, 17 (1921) 475.

[9] M.Borowski, Perovskite structure, properties and uses, (2010) 437.

[10] M. Demaeder, D. Damjanovic & N. Setter, "Lead-free piezoelectric materials"Journal of Electroceramics, 13, pp.385–392, (2004).

[11] T. Takenaka, Piezoelectric properties of some lead-free ferroelectric ceramics. Ferroelectrics, 230 (1999) 87.

[12] A diffuse phase transition study on $Ba2^{+}$ substituted NBT ferroelectric ceramic. K.Rao,B.Tilak,K.Ch,A.S,H.Workineh 509 (2011) 7121-7129

[13] Additive effects on electrical properties of NBT ferroelectric ceramics.H.Nagata,T.Takenaka. 21 (2001) 1299-1302.

[14] Zhou, W. W. Peng, D. Zhang, X. Y. Yang and W. Chen, Polarization properties of Na1/2Bi1/2TiO3 system:First-principles calculation and experimental.Computational Materials Science, 44 (2008) 67.

[15] Dunmin Lin . Chenggang Xu. Qiaoji Zheng Yujun Wei. Daojiang Gao Y. Wang et al. J Mater Sci. Mater Electron (2009) 20:393–397

[16] Matjaz Valant,* Taras Kolodiazhnyi, Iztok Arcˇon, Frederic Aguesse, Anna-Karin Axelsson and Neil M. Alford, Adv. Funct. Mater. 2012, 22, 2114–2122

[17]. Sintering Densification, Grain Growth, and Microstructure Suk-Joong L. Kang (1-75)

[18] "Nanoparticle Compatibility: New Nanocomposite Processing Technique Creates More Powerful Capacitors". Retrieved 2009-06-06

[19] Solid State Physics R.K.Puri, V.K.Babber ISO 2000.

[20] Vapor Transport Sintering of Calcium Phosphate Ceramics (2012) 5-40

[21] B. D. Cullity, S. R. Stock, Elements of X-Ray Diffraction. (3rd Edition) Prentice Hall, (2001).

[22] An inexpensive, sensitive vibrating sample magnetometer

S R Hoon Eur. J. Phys. 4 (1983) 61-67

[23] Versatile and Sensitive Vibrating-Sample Magnetometer Foner RSI 30(1959)

[24] G. Cao, Nanostructures & nanomaterials Synthesis, Properties & Applications. Imperial College Press, (2004).

[25] W. A. Bonner and G. J. Zydzik, Growth of single crystal lead molybdate for acousto optic applications. Journal of Crystal Growth, 7 (1970) 65.